IEEE Open Journal of Vehicular Technology

Received 13 May 2025; accepted 29 May 2025. Date of publication 2 June 2025;
date of current version 23 June 2025. The review of this article was coordinated by Editor Chenhao Qi.

Digital Object Identifier 10.1109/OJVT.2025.3576062

Wavelet Transform Aided Single-Carrier FDMA With Index Modulation

ZHOU LU, MOHAMMED EL-HAJJAR (Senior Member, IEEE), AND LIE-LIANG YANG (Fellow, IEEE)

School of Electronics and Computer Science, University of Southampton, SO17 1BJ Southampton, U.K.

CORRESPONDING AUTHOR: LIE-LIANG YANG (e-mail: lly@ecs.soton.ac.uk).

This work was supported in part by Engineering and Physical Sciences Research Council (EPSRC) Projects under Grant EP/X01228X/1, Grant EP/X04047X/1, and Grant EP/Y037243/1 and in part by the Future Telecoms Research Hub, Platform for Driving Ultimate Connectivity (TITAN) through the Department of Science Innovation and Technology.

ABSTRACT Single-carrier frequency-division multiple access (SC-FDMA) is a well-known multiuser transmission method for uplink communications owing to its low peak-to-average power ratio (PAPR) characteristics. Simultaneously, index modulation (IM) has been widely studied owing to its flexibility for spectral-efficiency versus energy-efficiency trade-off. However, applying conventional IM schemes with SC-FDMA may affect the desirable characteristics of SC-FDMA signals, resulting in the increase of PAPR, for example. On the other side, Wavelet Transform (WT) has been shown to provide an improved performance over the fast Fourier transform (FFT)-based SC-FDMA, owing to WT's local focusing capability in both time and frequency domains. In this paper, we propose three IM schemes, namely Symbol Position Index Modulation (SPIM), Spreading Matrix Index Modulation (SMIM) and Joint Matrix-Symbol Index Modulation (JMSIM) schemes, which perform IM at the symbol vector level, spreading matrix level, or a combination of both. These IM schemes are implemented with the WT-based SC-FDMA for data transmission. We consider two spreading matrix design schemes, namely random dispersion matrix design and Gram-Schmidt (GS) orthogonalization matrix design. Correspondingly, we propose different detection schemes, including Maximum Likelihood Detection (MLD), Simplified Maximum Likelihood Detection (SMLD), and the Two Stage Index-QAM Detection (TSD). The performance of the proposed schemes is evaluated by simulations. Our studies and results show that all the three schemes can effectively reduce the PAPR encountered by the conventional IM-assisted SC-FDMA signals. Moreover, the method of GS matrices can provide a gain upto 20 dB compared with the method of random dispersion matrices. Furthermore, the GS-based system can employ the proposed low-complexity TSD, allowing to achieve a similar bit error rate (BER) performance as MLD, while requiring significantly low complexity.

INDEX TERMS Wavelet, OFDM, single carrier-frequency division multiple access (SC-FDMA), index modulation, spatial modulation, peak-to-average power ratio, detection.

I. INTRODUCTION

In recent years, with the expanding adoption of technologies such as the Internet of Things (IoT) and smart homes, wireless communication has been increasingly required to support a variety of applications and services [1]. This has led to a significant rise in the demand for accommodating higher data rates and a growing number of users and connected nodes [2]. Orthogonal frequency-division multiple-access (OFDMA), as a variant of the famous orthogonal frequency-division multiplexing (OFDM), allows multiple users to share communication resources and hence, is one of the key multiple access techniques used in wireless communications [3]. OFDMA is characterized by high spectral efficiency, fast data transmission and low error rate, while resulting in a high peak to average power ratio (PAPR) due to its multi-carrier modulation (MCM) characteristics, which imposes heavy demand on the digital-to-analog convertors (DACs) and analog-to-digital convertors (ADCs) of transceivers [4], [5]. To mitigate the PAPR problem, in mobile wireless systems, single-carrier frequency-division multiple access (SC-FDMA) utilizing only

a portion of the available bandwidth to transmit a user's data has been introduced for uplink transmission, which has a reduced PAPR compared to OFDMA [6], [7], [8]. Specifically, the interleaved FDMA (IFDMA), one of the SC-FDMA schemes, evenly distributes user's data over the available bandwidth, resulting in a uniform power distribution and the PAPR can be reduced to the level of the single-carrier signaling schemes [9], [10], [11], [12], [13].

Conventional SC-FDMA-aided systems rely on fast Fourier transform (FFT) for data modulation, which generates the side-lobes that are only about 13 dB below the main lobe [14]. This makes the FFT-aided modulation schemes vulnerable to adjacent channel interference and lead to high out-of-band radiation (OOB). Instead of FFT, it has been shown that multi-carrier modulation implemented by discrete wavelet transform (DWT) can provide some benefits, including improved bit error rate (BER) performance, lower PAPR, higher spectral efficiency owing to the absence of cyclic prefix (CP) and higher immunity against carrier frequency offsets (CFOs) [15], [16], [17].

On the data modulation side, index modulation (IM) using indices as degrees of freedom for information transmission has received intensive research in recent years [18]. To implement IM, the indices can be embedded in spatial domain, time-domain or frequency-domain, or a combination of these [19], [20], [21], [22], [23], [24], [25]. Specifically, in spatial domain, indices can be defined according to the transmit antennas or receive antennas to form the so-called spatial modulation (SM) [26], [27], [28]. In time-domain, indices can be defined on time slots to allow transmission in a time-hopping mode [22], [29]. In frequency-domain, indices can be defined in terms of subcarriers, and hence, it is feasible to implement IM with OFDM-based systems [30], [31], [32]. Generally, the studies on IM show that it has the characteristics of high power efficiency, low mutual interference, and simple hardware and detection requirements. Recently, IM has also been studied in the context of the reflective intelligent surfaces (RIS) and underwater acoustic communications [33], [34], [35]. Specifically, in [33], extra bits are implicitly transmitted via the joint exploitation of reference signals, RIS phases and subcarrier indices, thereby enhancing the throughput and spectral efficiency of RIS-assisted communication systems. Considering underwater communications, in [34], the IM based on subcarrier activation patterns and the indices of Hartley codes allows the energy- and correlation-based noncoherent detections, enabling to improve system's robustness and energy efficiency. Moreover, as demonstrated in [35], the resistance of chaotic signals to eavesdropping can be enhanced through block interleaving and RIS-phase indexing in the RIS-aided secure communication systems.

However, in the state-of-the-art literature, most of the IM-OFDM-based systems consider point-to-point transmissions, while wireless systems are usually expected to support multiple users. Furthermore, the conventional IM schemes for OFDM and SC-FDMA focus mainly on the performance of BER and spectral efficiency [36], [37]. In contrast, the potential effect of IM on the PAPR of SC-FDMA systems [38] is often overlooked. Therefore, in this paper, we apply IM in the wavelet transform (WT)-based SC-FDMA systems to support multi-user communications. To circumvent the PAPR problem, our proposed design of IM schemes aims to maintain the original characteristics, like low PAPR, of SC-FDMA signals. Explicitly, the indices of our proposed IM design can be based on data symbols' positions, which we refer to as the symbol position index modulation (SPIM) scheme, or on the spreading matrices, which we denote as the spreading matrix index modulation (SMIM) scheme, or on the joint SPIM and SMIM, referred to as the JMSIM. Hence, the novel contributions of this paper can be summarized as follows:

- We propose three IM schemes, namely SPIM, SMIM and JMSIM, for operation with the WT-based SC-FDMA scheme. These IM schemes are applied before the conventional SC-FDMA scheme, to mitigate the increase in PAPR typically caused by the traditional IM schemes operated at subcarrier level.
- We propose two methods to design the spreading matrices used for the proposed schemes, namely the random dispersion matrices and Gram-Schmidt (GS) orthogonalization matrices, whose performance is studied in the context of the three proposed IM schemes. The results demonstrate that the GS method can provide better BER performance than the random dispersion matrices method, at least 20 dB at a BER of 10^{-4} in the SPIM scenario. The maximum gain can be attained by the JMSIM scheme with GS method, which is about 25 dB at a BER of 10^{-4} compared with that by the JMSIM scheme with the method of random dispersion matrices.
- We propose a low-complexity signal detection method, namely two stage index-QAM detection (TSD), for the proposed schemes, which is compared with two higher complexity benchmark detection methods, i.e., the maximum likelihood detection (MLD) and the simplified maximum likelihood detection (SMLD). Simulation results show that the low-complexity detection method can achieve a BER performance close to that of the high-complexity detection methods, when matrices are designed using the GS method. For example, the complexity of the proposed TSD is, respectively, about 30, which is two times lower than the complexity of the two benchmark detection methods in the SPIM scheme.

The rest of this paper is organized as follows. Section II introduces the proposed WT-based SC-FDMA and the three proposed IM schemes, namely SPIM, SMIM and JMSIM, followed by a discussion of the WT, the proposed subcarrier mapping methods and the designs of random dispersion matrices and Gram-Schmidt (GS) orthogonalization matrices. Section III introduces the maximum likelihood detection (MLD), simplified maximum likelihood detection (SMLD) and the two stage index-QAM detection (TSD) with SPIM, SMIM and JMSIM schemes. Section IV compares the performances of the three schemes with different detection methods and Section V provides our conclusions.

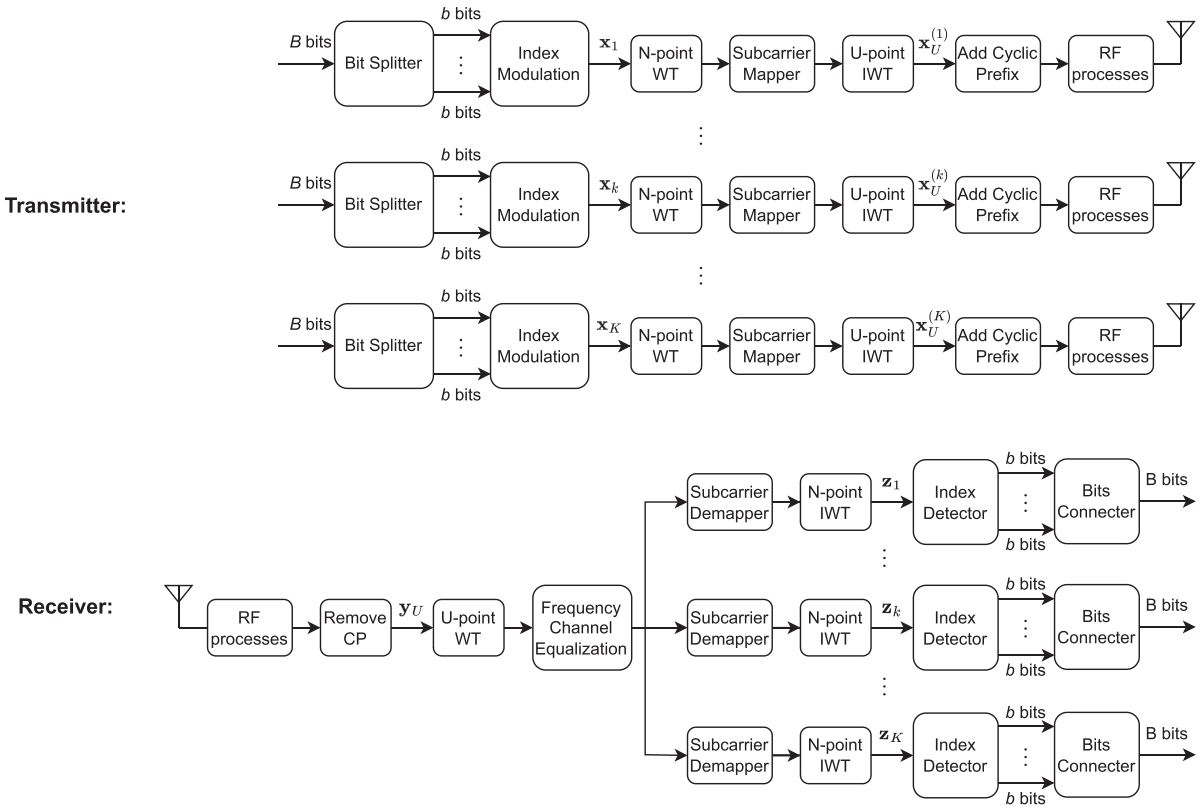

FIGURE 1. Transceiver diagram of the proposed uplink SC-FDMA.

II. SYSTEM MODEL

This section introduces an uplink SC-FDMA system incorporating WT and IM. At the transmitter side, the bit streams are divided into two parts: one for IM and the other for QAM/PSK modulation, forming symbol vectors. Following WT, the frequency-domain symbols are mapped onto subcarriers and subsequently converted back to the time-domain by inverse WT (IWT) for transmission. The signals, after traversing the frequency-selective fading channel, are then observed by a receiver. In contrast to the conventional IM methods that apply indices directly to subcarriers, the multiuser scheme currently considered implements IM outside the SC-FDMA structure with the assistance of a spreading matrix. This structure effectively mitigates the PAPR increase possibly associated with IM, enabling the system to retain low PAPR inherent to the conventional SC-FDMA.

A. TRANSMISSION MODEL

Fig. 1 shows the block diagram of the proposed uplink SC-FDMA system. Assume that a SC-FDMA system uses a total of U subcarriers to support the transmission of K users. Each user is assigned N subcarriers, hence $U = KN$. Each OFDM symbol consists of B bits, which are separated into two parts for IM and symbol modulation, respectively. After the IM process, the N-length symbol vector $\boldsymbol{x}_k$ for user k is obtained. Note that IM schemes will be introduced in detail in Section II-D.

As shown in Fig. 1, WT is implemented to transfer $\boldsymbol{x}_k$ from time-domain to frequency-domain for subcarrier mapping. Let the signal after WT be expressed as

$$\boldsymbol{X}_k = \boldsymbol{\mathcal{W}}_N \boldsymbol{x}_k = [X_k(0), X_k(1), \ldots, X_k(N-1)]^T, \quad (1)$$

where $\boldsymbol{\mathcal{W}}_N$ donates an N-point WT matrix [39]. Then, the symbols in $\boldsymbol{X}_k$ are mapped to N out of the U subcarriers, expressed as

$$\boldsymbol{X}_U^{(k)} = \boldsymbol{P}_k \boldsymbol{X}_k, \quad (2)$$

where $\boldsymbol{P}_k$ is the subcarrier mapping matrix satisfying the property $\boldsymbol{P}_k^T \boldsymbol{P}_k = \boldsymbol{I}_N$ for the subcarrier mapping. Finally, the symbol vector $\boldsymbol{X}_U^{(k)}$ is transformed back to the time-domain by the IWT, yielding

$$\boldsymbol{x}_U^{(k)} = \boldsymbol{\mathcal{W}}_U^H \boldsymbol{X}_U^{(k)}, \quad (3)$$

which is a $U \times 1$ vector. In (3), $[\cdot]^H$ denotes the conjugate transpose operation. Then, by following the principle of SC-FDMA, after adding the cyclic prefix (CP) to protect the signal from inter-symbol interference (ISI) due to the multipath effects, the signal is sent to the receiver through the wireless channel.

Assume that signals are transmitted over frequency-selective fading channels, with the time-domain channel impulse response (CIR) expressed as

$$\boldsymbol{h}_T^{(k)} = \left[h_0^{(k)}, h_1^{(k)}, \ldots, h_{L-1}^{(k)}\right]^T, \quad k = 1, 2, \cdots K, \quad (4)$$

where L is the number of taps. Then, the channel matrix $\boldsymbol{H}_k$ in the time-domain is given by

$$\boldsymbol{H}_k = \sum_{l=0}^{L-1} h_l^{(k)} \boldsymbol{\Pi}^l, \quad k = 1, 2, \cdots K, \tag{5}$$

where $\boldsymbol{\Pi}^l$ is the forward cyclic shift matrix obtained by shifting the $U \times U$ identity matrix left l times. The received signal in the time-domain can be expressed as

$$\boldsymbol{y}_U = \sum_{k=1}^{K} \boldsymbol{H}_k \boldsymbol{x}_U^{(k)} + \boldsymbol{n}, \tag{6}$$

where $\boldsymbol{n}$ denotes the Gaussian noise, which obeys the complex Gaussian distribution of $\mathcal{CN}(0, \sigma^2 \boldsymbol{I}_U)$, where σ^2 is the noise variance.

As shown in Fig. 1, following the principles of SC-FDMA, the cyclic prefix is removed first at receiver. Then, a U-point WT is applied to transfer the signal from time-domain to frequency-domain for channel equalization. The frequency-domain output signals are obtained by

$$\begin{aligned} \boldsymbol{Y}_U &= \boldsymbol{\mathcal{W}}_U \boldsymbol{y}_U \\ &= \boldsymbol{\mathcal{W}}_U \sum_{k=1}^{K} \boldsymbol{H}_k \boldsymbol{\mathcal{W}}_U^H \boldsymbol{X}_U^{(k)} + \boldsymbol{n}' \\ &= \sum_{k=1}^{K} \boldsymbol{H}_{eq}^k \boldsymbol{X}_U^{(k)} + \boldsymbol{n}', \quad k = 1, 2, \cdots K, \end{aligned} \tag{7}$$

where $\boldsymbol{H}_{eq}^{(k)} \triangleq \boldsymbol{\mathcal{W}}_U \boldsymbol{H}_k \boldsymbol{\mathcal{W}}_U^H$ is the equivalent channel matrix in the frequency-domain for the kth user and $\boldsymbol{n}' \triangleq \boldsymbol{\mathcal{W}}_U \boldsymbol{n}$ is the corresponding Gaussian noise.

Based on the different equalization methods in the principles of matched-filtering (MF), zero-forcing (ZF) and minimum mean square error (MMSE) [40], [41], the channel equalization matrix can be expressed as

$$\boldsymbol{W}_{MF}^{(k)} = \boldsymbol{H}_{eq}^{(k)}, \tag{8}$$

$$\boldsymbol{W}_{ZF}^{(k)} = \boldsymbol{H}_{eq}^{(k)} \left[(\boldsymbol{H}_{eq}^{(k)})^H \boldsymbol{H}_{eq}^{(k)} \right]^{-1}, \tag{9}$$

$$\boldsymbol{W}_{MMSE}^{(k)} = \boldsymbol{H}_{eq}^{(k)} \left[(\boldsymbol{H}_{eq}^{(k)})^H \boldsymbol{H}_{eq}^{(k)} + \sigma^2 \boldsymbol{I}_U \right]^{-1}. \tag{10}$$

The equalized signal $\boldsymbol{Z}_U^{(k)}$ can be represented as

$$\boldsymbol{Z}_U^{(k)} = \left(\boldsymbol{\Delta}^{(k)} \right)^{-1} \left(\boldsymbol{W}^{(k)} \right)^H \boldsymbol{Y}_U, \tag{11}$$

where $\boldsymbol{\Delta}^{(k)}$ is a diagonal matrix to make the diagonal elements of $(\boldsymbol{\Delta}^{(k)})^{-1} (\boldsymbol{W}^{(k)})^H \boldsymbol{H}_{eq}^{(k)}$ equal to one, which can be obtained as $\boldsymbol{\Delta}^{(k)} = \text{diag}((\boldsymbol{W}^{(k)})^H \boldsymbol{H}_{eq}^{(k)})$, where $\text{diag}(\boldsymbol{A})$ returns a diagonal matrix with the same diagonal elements as $\boldsymbol{A}$.

After the channel equalization, the subcarrier demapping is carried out by multiplying the transpose matrix of $\boldsymbol{P}_k$, to obtain the frequency-domain signals of user k as

$$\boldsymbol{Z}_k = \boldsymbol{P}_k^T \boldsymbol{Z}_U^{(k)}, \quad k = 1, 2, \ldots, K. \tag{12}$$

Finally, applying the N-point IWT, the observations for user k are given by

$$\boldsymbol{z}_k = \boldsymbol{\mathcal{W}}_N^H \boldsymbol{Z}_k, \tag{13}$$

based on which the index and M-QAM/PSK symbols are detected, as detailed in forthcoming discourses.

Note that, compared with the MF and MMSE schemes, the detection with the ZF scheme experiences no interference. This can be seen when substituting (5), (6) and (9) into (11), and then completing (12) and (13), which yields

$$\boldsymbol{z}_k = \boldsymbol{x}_k + \boldsymbol{n}_k. \tag{14}$$

Otherwise, when MF or MMSE is employed, there still exists no multiuser interference, as different users transmit information on different subcarriers. However, intra-user interference may exist, as the result of MF or MMSE processing.

B. WAVELET TRANSFORM

In the conventional SC-FDMA systems, signal is transformed from time-domain to frequency-domain by FFT. After subcarrier mapping or demapping, signal is then transformed back to time-domain. In this process, the Fourier transform, i.e., FFT, decomposes a signal into sine and cosine waves that extend infinitely in time. While this approach provides comprehensive global information about the signal in frequency-domain, it fails to capture variations at specific time points. Consequently, FFT is unable to accurately identify the timing of changes when a signal exhibits time-varying behavior or abrupt transitions [42].

In contrast, WT employs wavelets, with finite time support as basis functions. By translating and scaling these wavelets, WT facilitates localized analysis of signals in both time- and frequency-domains. This enables WT not only to identify the frequency components of a signal but also to pinpoint their precise temporal locations, achieving simultaneous localization in time and frequency. This unique capability makes WT particularly advantageous for analyzing non-stationary signals, detecting transient events, and examining local signal features, offering distinct benefits over the traditional FFT methods [43]. More specifically, the signal decomposition using WT is achieved by filter banks, each of which contains a low-pass filter (LPF) and a high-pass filter (HPF). Assume $\boldsymbol{x}[n]$ is the input signal containing both high and low-frequency components. The components are decomposed by passing the signal through a LPF $g[n]$ and a HPF $h[n]$. To satisfy the Nyquist Theorem, both components are up-sampled by two. The high-frequency components are set aside as the input to the next level, where the low- and high-frequency components are again decomposed until the last level. Note that, WT has various kinds of bases [44] to suit different needs. In this paper, we choose the Haar wavelet [44] as the basis of WT. The Haar wavelet is characterized by its mathematical simplicity and computational efficiency, enabling rapid processing and analysis of signals. It is particularly effective in capturing local features and abrupt changes within signals. Furthermore, its orthogonality and compact

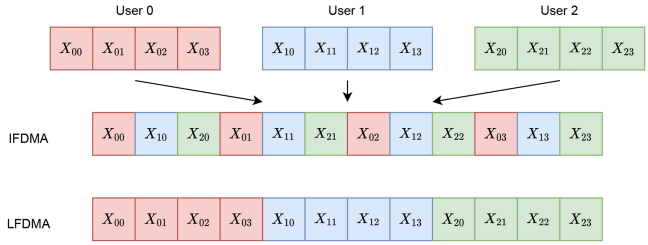

FIGURE 2. Subcarrier mapping for IFDMA and LFDMA.

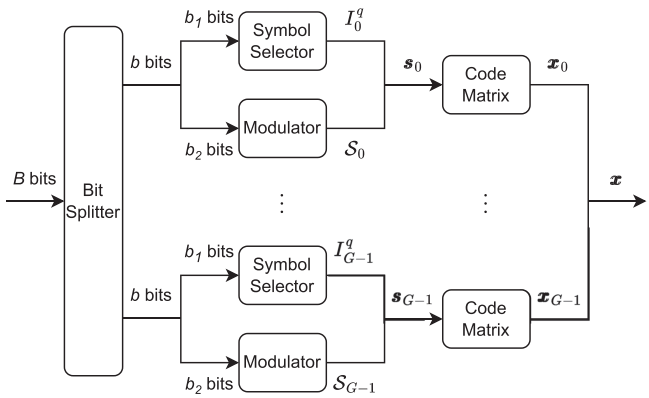

FIGURE 3. Symbol position index modulation (SPIM).

support properties contribute to its outstanding performance in applications for, such as, signal processing and image analysis.

C. SUBCARRIER MAPPING/DEMAPPING

With SC-FDMA, there are two methods suggested to map the symbols after DFT onto subcarriers, yielding interleaved frequency division multiple access (IFDMA) and localized frequency division multiple access (LFDMA) [45]. For example, assume that there is an SC-FDMA structure with a total $U = 12$ subcarriers, $K = 3$ users and each user uses $N = 4$ subcarriers, as shown in Fig. 2. In IFDMA, the symbols for all users are distributed evenly over the entire frequency band. By contrast, in LFDMA, all symbols of the same user are mapped to adjacent subcarriers, which leads to a higher PAPR in comparison with IFDMA [45]. Therefore, in this paper, we choose the mapping method of IFDMA to map users' data symbols to subcarriers.

D. INDEX MODULATION SCHEMES

In this subsection, three IM schemes are introduced by applying the indices of symbol positions, spreading matrices or both of them, which we refer to as SPIM, SMIM and JMSIM, respectively.

1) SYMBOL POSITION INDEX MODULATION (SPIM)

Fig. 3 shows the block diagram of SPIM, where the B bits of a user are divided into G groups with b bits per group, i.e. $B = bG$, where b bits of a group are separated into two parts, expressed as $b = b_1 + b_2$, for IM and symbol modulation, respectively. Specifically, b_1 bits generate an index q to select a symbol position pattern I_q from the possible patterns in the set $\mathcal{I} = \{I_0, I_1, \ldots, I_{Q-1}\}$, where I_q represents a symbol position pattern obtained by activating n out of $N_g = N/G$ symbol positions. Hence, the position set $\mathcal{I}$ is a subset of the initial index set expressed as

$$\mathcal{I}_{\text{ini}} = \left\{I_0, I_1, \ldots, I_q, \ldots, I_{C_{N_g}^n - 1}\right\}, \tag{15}$$

where $C_{N_g}^n$ is the total number of combinations of selecting n from N_g symbol positions. Consequently, we have $Q = 2^{b_1} \leq C_{N_g}^n$. The remaining b_2 bits in a b-bit symbol generate for each group a symbol set $\mathcal{S}_g = \{S_0, S_1, \cdots\}$ based on M-QAM/PSK modulation, where $S_i \in \mathcal{M}$ with $\mathcal{M}$ containing the M possible M-QAM/PSK symbols. Then, the symbols in $\mathcal{S}_g$ are mapped to form the signal vector $\boldsymbol{s}_g$ of length N_g, which can be expressed as

$$\boldsymbol{s}_g = \left[s_0, s_1, \ldots, s_{N_g-1}\right]^T, \quad g = 0, 1, \ldots, G-1, \tag{16}$$

where $[\cdot]^T$ denotes the transpose operation. In (16), the N_g length symbol vector $\boldsymbol{s}_g$ consists of two types of symbols, i.e. the symbols from $\mathcal{S}_g$ of M-QAM/PSK symbols and symbol "0" representing inactive symbols. Hence, according to the application of the IM on the positions of modulated symbols from $\mathcal{S}_g$ or "0", two mapping schemes are considered, called the 'On' mapping (ONM) and 'Off' mapping (OFM), which enhances the flexibility of IM.

a) "On" Mapping: With ONM, the data symbols in $\mathcal{S}_g$ are mapped to the selected n positions in the symbol position pattern I_q, and the rest are set to "0", representing the inactive symbols. Hence, there are n symbols in $\mathcal{S}_g$, in the form of

$$\mathcal{S}_{g(on)} = \{S_0, S_1, \ldots, S_{n-1}\} \subset \mathcal{M}^n. \tag{17}$$

Accordingly, the number of bits conveyed by the M-QAM/PSK modulation per group is

$$b_{2(on)} = n \log_2(M). \tag{18}$$

b) "Off" Mapping: In the context of OFM, "0"s are mapped to the selected n positions in I_q, while the rest are for the M-QAM/PSK symbols. Hence, there are $(N_g - n)$ symbols in $\mathcal{S}_g$, having the form of

$$\mathcal{S}_{g(off)} = \{S_0, S_1, \ldots, S_{N_g-n-1}\} \subset \mathcal{M}^{N_g-n-1}. \tag{19}$$

Therefore, the number of bits conveyed by the M-QAM/PSK modulation per group is

$$b_{2(off)} = (N_g - n) \log_2(M). \tag{20}$$

Consequently, when considering one transmission of G groups of a user, the number of bits delivered by the symbol index patterns is

$$B_1 = Gb_1 = G \log_2(Q), \tag{21}$$

and the bits by the M-QAM/PSK symbols are

$$B_{2(on)} = Gb_{2(on)} = Gn \log_2(M), \tag{22}$$

when the ONM scheme is employed, or

$$B_{2(off)} = Gb_{2(off)} = G(N_g - n)\log_2(M), \tag{23}$$

when the OFM scheme is used. The total number of bits per transmission by a user is given by

$$\begin{aligned} B_{(on)} &= B_1 + B_{2(on)} \\ &= G(\log_2(Q) + n\log_2(M)) = G\log_2(QM^n), \end{aligned} \tag{24}$$

in the case of using ONM, or

$$\begin{aligned} B_{(off)} &= B_1 + B_{2(off)} \\ &= G(\log_2(Q) + (N_g - n)\log_2(M)) \\ &= G\log_2(QM^{N_g - n}), \end{aligned} \tag{25}$$

when the OFM is implemented.

After obtaining the symbol vector $\boldsymbol{s}_g$ for each group, as shown in Fig. 3, multiplying the code matrix $\boldsymbol{A}$ gives

$$\boldsymbol{x}_g = \boldsymbol{A}\boldsymbol{s}_g, \qquad g = 0, 1, \ldots, G-1, \tag{26}$$

where, for the sake of reducing detection complexity at receiver side, the code matrix $\boldsymbol{A}$ is desirable to be an orthonormal matrix, satisfying

$$\boldsymbol{A}^H\boldsymbol{A} = \boldsymbol{I}_{N_g}, \tag{27}$$

with $\boldsymbol{I}_{N_g}$ is a $(N_g \times N_g)$ being an identity matrix. However, in dispersive channels, orthogonality may be hard to maintain. Hence, the design of code matrix $\boldsymbol{A}$ for SPIM as well as the code matrices used in SMIM and JMSIM will be considered in detail in Section II-E of this section.

Finally, $\boldsymbol{x}_g$ for $g = 0, 1, \ldots, G-1$ are combined to form a N-length vector as

$$\boldsymbol{x} = \left[\boldsymbol{x}_0^T, \boldsymbol{x}_1^T, \ldots, \boldsymbol{x}_{G-1}^T\right]^T, \quad \boldsymbol{x} \in \mathbb{C}^{N\times 1}, \tag{28}$$

which is further processed, such as WT, for transmission, as described in Section II-A.

2) SPREADING MATRIX INDEX MODULATION (SMIM)

Fig. 4 shows the block diagram of SMIM. Again, B bits of a user are split into G groups, each with b bits, i.e., $B = bG$. In each group, b bits are further divided into two parts, i.e., $b = b_1 + b_2$, where b_1 bits are used to generate an index q for selecting a spreading matrix $\boldsymbol{A}_q$ from the set $\mathcal{A}$

$$\mathcal{A} = \left\{\boldsymbol{A}_0, \boldsymbol{A}_1, \ldots, \boldsymbol{A}_q, \ldots, \boldsymbol{A}_{Q-1}\right\}, \tag{29}$$

where $Q = 2^{b_1}$. The matrices $\boldsymbol{A}_q$ are desirably near-orthogonal to each other, i.e., to satisfy the property $(\boldsymbol{A}_q)^H\boldsymbol{A}_q \approx \boldsymbol{I}$, in order to facilitate signal detection at the receiver. The b_2 bits generate the N_g M-QAM/PSK symbols. In the SMIM scheme, all symbol positions are activated for transmission of M-QAM/PSK symbols. Hence, the M-QAM/PSK symbol vector is expressed by

$$\boldsymbol{s}_g = \left[s_0, s_1, \ldots, s_{N_g-1}\right]^T. \tag{30}$$

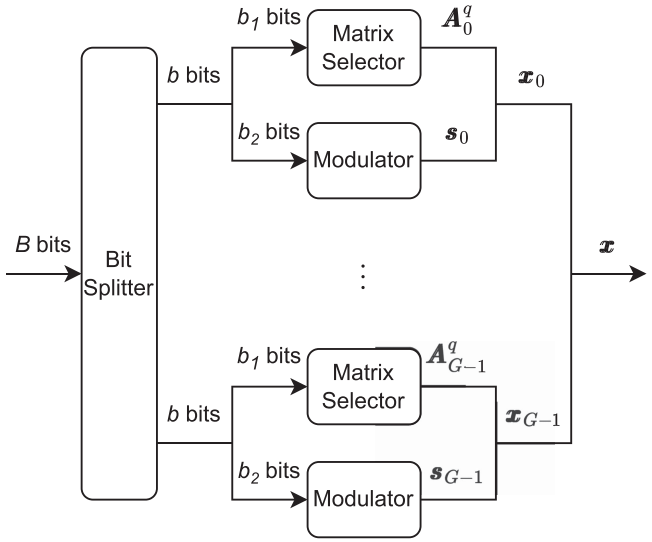

FIGURE 4. Spreading matrix index modulation (SMIM).

Consequently, the information signals of the gth group can be expressed as

$$\boldsymbol{x}_g = \boldsymbol{A}_{q,g}\boldsymbol{s}_g, \quad g = 0, 1, \ldots, G-1, \tag{31}$$

where $\boldsymbol{A}_{q,g}$ is the spreading matrix of group g chosen from $\mathcal{A}$.

From the above analysis, it can be seen that the total number of bits for spreading matrix selection is

$$B_1 = Gb_1 = G\log_2(Q), \tag{32}$$

while the total number of bits carried by M-QAM/PSK is

$$B_2 = Gb_2 = GN_g\log_2(M). \tag{33}$$

Hence, the total number of bits transmitted per OFDM symbol per user is

$$\begin{aligned} B = B_1 + B_2 &= G\left[\log_2(Q) + N_g\log_2(M)\right] \\ &= G\log_2\left(QM^{N_g}\right). \end{aligned} \tag{34}$$

3) JOINT MATRIX-SYMBOL INDEX MODULATION (JMSIM)

Fig. 5 illustrates the block diagram of JMSIM, where B bits are split into G groups with b bits in each group, hence $B = bG$. In each group, b bits are further divided into three parts for different sub-modulations: b_0 bits by the SMIM, b_1 bits by the SPIM and the remaining b_2 bits by the M-QAM/PSK, making $b = b_0 + b_1 + b_2$. Specifically, for SMIM, b_0 bits are used to select a spreading matrix $\boldsymbol{A}_{q_c,g}$ from the matrix set

$$\mathcal{A} = \left\{\boldsymbol{A}_0, \boldsymbol{A}_1, \ldots, \boldsymbol{A}_{q_c}, \ldots, \boldsymbol{A}_{Q_c-1}\right\}, \tag{35}$$

where $Q_c = 2^{b_0}$ and $\boldsymbol{A}_{q_c} \in \mathbb{C}^{N_g\times N_g}$. Here, again, the matrices are desirably near-orthogonal. For SPIM, b_1 bits are used to select a symbol position scheme $I_{q,g}$ from the symbol index set

$$\mathcal{I} = \left\{I_0, I_1, \ldots, I_q, \ldots, I_{Q_s-1}\right\}, \tag{36}$$

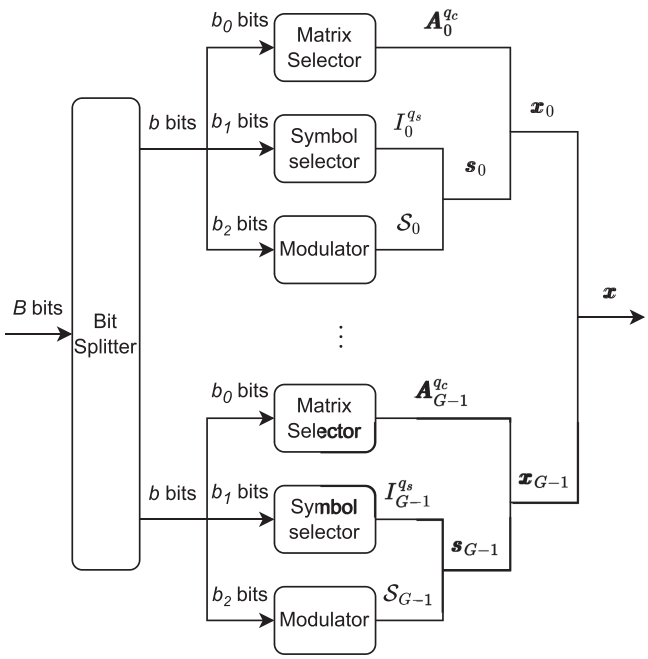

FIGURE 5. Joint matrix symbol index modulation (JMSIM).

which as (15), is obtained by choosing n out of N_g symbol positions, where $Q_s = 2^{b_1} \leq C_{N_g}^n$. Finally, the remaining b_2 bits are used to form the M-QAM/PSK symbols in the set $\mathcal{S}_g$ that are transmitted in conjunction with the indices. Consequently, after mapping the n symbols from $\mathcal{S}_g$ into a symbol vector $\boldsymbol{s}_g$ according to the symbol position scheme $I_{q,g}$, and applying the selected matrix $\boldsymbol{A}_{q_c,g}$, we obtain the processed data for the g-th group as

$$\boldsymbol{x}_g = \boldsymbol{A}_{q_c,g}\boldsymbol{s}_g. \tag{37}$$

Since the JMSIM scheme includes the SPIM scheme, "ONM" or "OFM" can be implemented. Hence, the total number of bits per symbol (BPS) conveyed by M-QAM/PSK is

$$B_{2(on)} = Gb_{2(on)} = Gn\log_2(M), \tag{38}$$

$$B_{2(off)} = Gb_{2(off)} = G(N_g - n)\log_2(M). \tag{39}$$

The total number of BPS by SPIM is

$$B_1 = Gb_1 = G\log_2(Q_s), \tag{40}$$

while the total number of BPS by SMIM is

$$B_0 = Gb_0 = G\log_2(Q_c). \tag{41}$$

Therefore, the total number of bits per OFDM symbol per user can be expressed as

$$B_{(on)} = B_0 + B_1 + B_{2(on)} = G\log_2(Q_cQ_sM^n), \tag{42}$$

$$B_{(off)} = B_0 + B_1 + B_{2(off)} = G\log_2(Q_cQ_sM^{N_g-n}). \tag{43}$$

Note that, in our SPIM scheme, index mapping can be implemented similarly as that in [46], [47]. Here is an example

TABLE 1. An Example to Explain the Index Mapping in SPIM With $N_g = 5$ and $b_1 = 3$

q	I_q with ONM	I_q with OFM
0	[1, 1, 0, 0, 0]	[0, 0, 1, 1, 1]
1	[1, 0, 1, 0, 0]	[0, 1, 0, 1, 1]
2	[1, 0, 0, 1, 0]	[0, 1, 1, 0, 1]
3	[1, 0, 0, 0, 1]	[0, 1, 1, 1, 0]
4	[0, 1, 1, 0, 0]	[1, 0, 0, 1, 1]
5	[0, 1, 0, 1, 0]	[1, 0, 1, 0, 1]
6	[0, 1, 0, 0, 1]	[1, 0, 1, 1, 0]
7	[0, 0, 1, 1, 0]	[1, 1, 0, 0, 1]

to show the index mapping in SPIM. Assume that the number of symbols per group is $N_g = 5$. Then, selecting 2 out of the 5 symbol positions can transmit $b_1 = 3$ bits. Hence, when considering the ONM and OFM schemes, the index mapping in SPIM can be shown as Table 1, where q is the decimal representation of 3 binary bits.

In SMIM, the mapping is straightforward. Assume that there are two candidate spreading matrices in $\mathcal{A}$, i.e., $\mathcal{A} = \{\boldsymbol{A}_0, \boldsymbol{A}_1\}$. Then, by activating one of the two spreading matrices, $b_0 = 1$ bit can be transferred per symbol by exploiting the two spreading matrices.

Finally, for JMSIM, if the above two examples are combined, we can readily know that $b_0 + b_1 = 4$ bits can be conveyed per symbol duration by jointly exploiting the 2 indices of spreading matrices and the 8 indices of symbol activation patterns as shown in Table 1.

For any of the three IM schemes, finally, the G groups of signals of a user are combined to form a N-symbol vector, expressed as

$$\boldsymbol{x} = \left[\boldsymbol{x}_0^T, \boldsymbol{x}_1^T, \ldots, \boldsymbol{x}_{G-1}^T\right]^T \in \mathbb{C}^{N\times 1}, \tag{44}$$

which is the input signal to the WT. Then, as seen in Fig. 1, the N outputs of WT are mapped to N out of the U subcarriers in frequency-domain. Then, it is transformed back to the time-domain by the IWT operation. These processings are given by the representations of (1)–(3).

E. DESIGN OF SPREADING MATRICES

In this subsection, we introduce some methods for spreading matrix design, including the dispersion matrices and orthogonal matrices. The spreading matrix is utilized in the SPIM scheme to mitigate PAPR before IM. In the SMIM and JMSIM schemes, the spreading matrices are directly applied to implement IM. For all the three schemes, the spreading matrices are unitary matrices to ensure efficient signal detection at receiver.

1) DISPERSION MATRICES

In the SMIM and JMSIM schemes, the spreading code matrices $\boldsymbol{A}_q \quad (q = 0, 1, \ldots, Q-1)$ affect the system performance significantly. Similar to the dispersion matrices in the

space-time shift-keying (STSK) modulation [48], the spreading matrices can be designed as follows. First, the matrices $\boldsymbol{A}_q (q = 0, 1, \ldots, Q-1)$ are randomly generated with each element following the Gaussian distribution and under the constraint of

$$\mathrm{tr}\left[(\boldsymbol{A}_q)^H \boldsymbol{A}_q\right] = N_g, \tag{45}$$

where tr[·] denotes the trace operation. Define $\mathcal{L}$ the set of all possible M-QAM/PSK symbol vectors $\boldsymbol{s}$ of N_g-length, which is expressed as

$$\mathcal{L} = \left\{\boldsymbol{s}_0, \boldsymbol{s}_1, \ldots, \boldsymbol{s}_{M^{N_g}-1}\right\}, \tag{46}$$

and let

$$\boldsymbol{\mathcal{C}} = [\boldsymbol{A}_0; \boldsymbol{A}_1; \cdots; \boldsymbol{A}_{Q-1}], \quad \boldsymbol{\mathcal{C}} \in \mathbb{C}^{N_g Q \times N_g}, \tag{47}$$

where $\boldsymbol{\mathcal{C}}$ represents the matrix containing Q dispersion matrices satisfying (45). Based on [48], [49], the Discrete-input Continuous-output Memoryless Channel (DCMC) capacity is given by

$$C = \frac{1}{N_g}\left(\log_2(N_g M) - \frac{1}{N_g M} \times \sum_{l} E\left[\log_2\left\{\sum_{l'} e^{\Psi_l^{l'}} \middle| \boldsymbol{s}_{l'}\right\}\right]\right), \tag{48}$$

where

$$\Psi_l^{l'} = -||\boldsymbol{H}\boldsymbol{\mathcal{C}}(\boldsymbol{s}_l - \boldsymbol{s}_{l'}) + \boldsymbol{n}||^2 + ||\boldsymbol{n}||^2, \tag{49}$$

and $\boldsymbol{H}$ and $\boldsymbol{n}$ are the channel matrix defined in Section II-A and the noise vector, respectively. It can be shown that C monotonically increases with the value of $\boldsymbol{\mathcal{C}}(\boldsymbol{s}_l - \boldsymbol{s}_{l'})$. Hence, the capacity is obtained by such a matrix $\boldsymbol{\mathcal{C}}$ that maximizes the difference between a signal $\boldsymbol{s}_l$ and any other signal $\boldsymbol{s}_{l'}$.

Therefore, the Q number of spreading code matrices $\{\boldsymbol{A}_q\}$ can be designed by a search process, which aims to obtain the C value of (48) as large as possible. Specifically, first, M_t sets of dispersion matrices, with each set containing Q dispersion matrices of required dimensions, are generated by the above-mentioned method for generating dispersion matrices. Then, for each set, the C value is calculated using (48). Finally, from the M_t sets, the set of Q dispersion matrices yielding the largest C value is selected for use in the SMIM or JSMIM. Note that, if N_g is large, it can be expected that a set of randomly generated Gaussian dispersion matrices is near-optimum, owing to the principles of massive multiple-input multiple-output (mMIMO) [50].

2) GRAM-SCHMIDT MATRICES

With the Gram-Schmidt (GS) orthogonalization [51], a random Gaussian matrix can be transformed to a unitary matrix without the limitation of size. In detail, let an initially generated $(N_g \times N_g)$ Gaussian matrix $\boldsymbol{A}$ be given by

$$\boldsymbol{A} = [\boldsymbol{a}_0, \boldsymbol{a}_1, \ldots, \boldsymbol{a}_{N_g-1}], \tag{50}$$

where $\boldsymbol{a}_n \in \mathbb{C}^{N_g \times 1}$ is the n-th column of $\boldsymbol{A}$. Assume that $\boldsymbol{P} = [\boldsymbol{p}_0, \boldsymbol{p}_1, \cdots, \boldsymbol{p}_{N_g-1}]$ is the orthogonal matrix derived from the GS orthogonalization. For the first column, corresponding to $n = 0$, $\boldsymbol{p}_0$ is equal to the normalized $\boldsymbol{a}_0$, i.e., $\boldsymbol{p}_0 = \boldsymbol{a}_0/|\boldsymbol{a}_0|$. For the remaining columns, i.e., for $n = 1, 2, \ldots, N_g - 1$, first, $\boldsymbol{v}_n$ is calculated from the formula

$$\boldsymbol{v}_n = \boldsymbol{a}_n - \sum_{j=1}^{n-1}\left(\frac{(\boldsymbol{p}_j \cdot \boldsymbol{a}_n)}{\|\boldsymbol{p}_j\|^2} \times \boldsymbol{p}_j\right). \tag{51}$$

Then, $\boldsymbol{p}_n$ is obtained from the normalization of $\boldsymbol{v}_n$, given by $\boldsymbol{p}_n = \boldsymbol{v}_n/|\boldsymbol{v}_n|$.

III. SIGNAL DETECTION

As introduced in Section II, there are three methods to implement IM with the WT-assisted SC-FDMA, namely SPIM, SMIM and the JMSIM obtained by combining SPIM and SMIM schemes. In this section, we introduce the detectors for the proposed schemes, which include the maximum likelihood detector (MLD), the proposed simplified MLD (SMLD) and the proposed low-complexity two-stage IM-QAM detector (TSD). The detection methods for the SPIM and SMIM modulated SC-FDMA will be introduced in detail, while the detector for the JMSIM-assisted SC-FDMA is the joint method of that used in the SPIM and SMIM cases.

A. MAXIMUM LIKELIHOOD DETECTION (MLD)

MLD works by considering all the possible combinations of the activated symbol positions and constellation points in SPIM scheme, or all the possible combinations of index matrices and symbol vectors in SMIM scheme.

1) MLD FOR SPIM

After the typical receiver processing following SC-FDMA, as described in Section II-A, the time-domain observations for one user is given by (13). Then, upon expressing $\boldsymbol{z}_k$, $k = 1, 2, \ldots, K$, in the form of G groups, $\boldsymbol{z}$ can be written as

$$z = \left[z_0^T, z_1^T, \ldots, z_{G-1}^T\right]^T, \tag{52}$$

where the subscript k for user indexing is ignored for simplicity. Following the principles of SPIM as detailed in Section II-D, the observation for the gth group can be expressed as

$$\begin{aligned} z_g &= \boldsymbol{s}_g + \tilde{\boldsymbol{n}}_g, \\ &= \boldsymbol{A}^H \boldsymbol{x}_g + \tilde{\boldsymbol{n}}_g, \quad g = 0, 1, \ldots, G-1, \end{aligned} \tag{53}$$

where $\boldsymbol{s}_g$ is the symbol vector corresponding to that transmitted by group g, which is obtained after removing the effect of the code matrix $\boldsymbol{A}$ applied on the transmitted signal $\boldsymbol{x}_g$. $\tilde{\boldsymbol{n}}_g$ is the Gaussian noise of group g after the receiving processing. MLD makes a joint detection of the activated symbol positions and constellation points by solving a minimization problem described as

$$\left(\hat{q}, \hat{\mathcal{S}}_g\right) = \underset{q \in \mathcal{Q}, \mathcal{S}_g \subset \mathcal{M}^\times}{\arg\min} ||z_g - \boldsymbol{s}_q||^2, \tag{54}$$

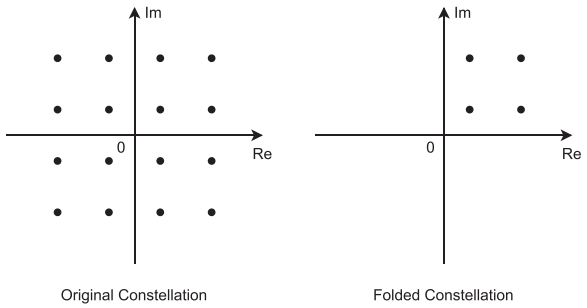

FIGURE 6. 16QAM constellation diagram folded for SMLD.

where, by definition, $\mathcal{Q} = \{0, \ldots, Q-1\}$, $\times$ is either n if ONM is employed, or $(N_g - n - 1)$ if OFM is employed. $\boldsymbol{s}_q$ is a possible combination of the activated symbol positions I_q and constellation points in set $\mathcal{S}_g$. At the end, $\hat{q}$ and $\hat{\mathcal{S}}_g$ are respectively the detected index symbol and the set of M-QAM/PSK symbols.

2) MLD FOR SMIM

In the SMIM-assisted SC-FDMA systems, after the receiver processing following SC-FDMA, the time-domain observations for the gth group can be expressed as

$$\boldsymbol{z}_g = \boldsymbol{A}_{q,g}\boldsymbol{s}_g + \tilde{\boldsymbol{n}}_g, \quad g = 0, 1, \ldots, G-1, \tag{55}$$

where $\boldsymbol{A}_q$ and $\boldsymbol{s}_g$ are respectively the activated index matrix and the transmitted symbol vector of group g, while $\tilde{\boldsymbol{n}}_g$ is the noise of group g after the receiving processing. The same as in the SPIM, the MLD in the SMIM-assisted SC-FDMA makes a joint decision on the activated index matrix and symbol vector by solving the following minimization problem:

$$(\hat{q}, \hat{\boldsymbol{s}}_g) = \underset{q\in\mathcal{Q}, \boldsymbol{s}_p \in \mathcal{M}^{N_g}}{\arg\min} ||\boldsymbol{z}_g - \boldsymbol{A}_{q,g}\boldsymbol{s}_p||^2, \tag{56}$$

yielding the detected index symbol $\hat{q}$ and a vector $\hat{\boldsymbol{s}}_g$ of N_g M-QAM/PSK symbols.

Although MLD provides optimal performance in noisy environments, its high computational complexity poses challenges for supporting the detection of large-scale data transmissions. To address this issue, we propose a simplified MLD method that decreases the total number of possible symbol combinations by folding the constellation diagram of the modulated symbols, thereby reducing the detection complexity.

B. SIMPLIFIED MLD (SMLD)

The main point of SMLD is to simplify the MLD by folding the constellation diagram [52]. To achieve this objective, the modulation constellation must be symmetric about the coordinate axes. Fig. 6 shows an example of folding the constellation points of 16QAM into the first quadrant, resulting in the constellation diagram for implementing SMLD with the corresponding points shown in Table 2. After folding, the coordinates of all points in the constellation diagram are positive or 0 (if the points are on the coordinate axes). Let us express $\mathcal{S}_{g,fold}$ the set of folded constellation points.

TABLE 2. Constellation Points in Original and Folded Constellation Diagram of 16QAM

Points in original constellation				Points in folded constellation
$1+i1$	$-1+i1$	$-1-i1$	$1-i1$	$1+i1$
$1+i3$	$-1+i3$	$-1-i3$	$1-i3$	$1+i3$
$3+i1$	$-3+i1$	$-3-i1$	$3-i1$	$3+i1$
$3+i3$	$-3+i3$	$-3-i3$	$3-i3$	$3+i3$

1) SMLD FOR SPIM

Using the points in the folded constellation, a new joint symbol book $\boldsymbol{s}_{fold}$ for MLD can be generated. Accordingly, the signs of both real and imaginary parts for all the complex symbols in $\boldsymbol{z}_g$ are converted to positive to get a new observation vector $\boldsymbol{z}_{g,fold}$, i.e., $\boldsymbol{z}_{g,fold}(n) = |\Re(\boldsymbol{z}_g(n))| + i|\Im(\boldsymbol{z}_g(n))|$ for each element of $\boldsymbol{z}_g$. Based on the folded observation, the SMLD is implemented as

$$(\hat{q}, \hat{\mathcal{S}}_{g,fold}) = \underset{q\in\mathcal{Q}, \mathcal{S}_{q,fold}\subset\mathcal{M}^{\times}_{1/4}}{\arg\min} ||\boldsymbol{z}_{g,fold} - \boldsymbol{s}_{fold}||^2, \tag{57}$$

where $\boldsymbol{s}_{fold}$ is a folded symbol vector obtained according to I_q and $\mathcal{S}_{q,fold}$, $\mathcal{M}_{1/4}$ is the set obtained from folding of $\mathcal{M}$, the size of $\mathcal{M}_{1/4}$ is 1/4 of that of $\mathcal{M}$. Again, in (57), $\times$ is either n if ONM is employed, or $(N_g - n - 1)$ if OFM is employed. As shown in Table 2, each folded symbol is mapped to 4 possible M-QAM symbols. To obtain the estimate to the actually transmitted one, for a folded symbol in $\hat{\mathcal{S}}_{g,fold}$, say $\hat{S}_{n,fold}$, a corresponding M-QAM symbol can be recovered as

$$\begin{aligned}\hat{S}_{n,fold} = {} & \text{sign}\left(\Re(\boldsymbol{z}_g(n))\right) \times \Re\left(\hat{S}_{n,fold}\right) \\ & + i \cdot \text{sign}\left(\Im(\boldsymbol{z}_g(n))\right) \times \Im\left(\hat{S}_{n,fold}\right)\end{aligned} \tag{58}$$

where sign(x) returns the sign of real value x.

Comparing (54) with (57), explicitly, the complexity of SMLD is 1/4 of MLD.

2) SMLD FOR SMIM

The symbol book $\boldsymbol{s}_{fold}$ for SMLD is the same as that used in the SPIM by folding the original constellation diagram, for example, as shown in Table 2. Then, according to the property of the spreading matrices, we can use

$$\boldsymbol{Z} = \left[\boldsymbol{A}_0 \boldsymbol{A}_1 \cdots \boldsymbol{A}_q \cdots \boldsymbol{A}_{Q-1}\right], \quad \boldsymbol{Z} \in \mathbb{C}^{N_g \times N_g Q}, \tag{59}$$

to remove the effect of the index matrix to obtain

$$\hat{\boldsymbol{z}} = \boldsymbol{Z}^H \boldsymbol{z}_g = \begin{bmatrix} \boldsymbol{A}_0^H \left(\boldsymbol{A}_{q,g}\boldsymbol{s}_g + \tilde{\boldsymbol{n}}_g\right) \\ \vdots \\ \boldsymbol{A}_q^H \left(\boldsymbol{A}_{q,g}\boldsymbol{s}_g + \tilde{\boldsymbol{n}}_g\right) \\ \vdots \\ \boldsymbol{A}_{Q-1}^H \left(\boldsymbol{A}_{q,g}\boldsymbol{s}_g + \tilde{\boldsymbol{n}}_g\right) \end{bmatrix} = \begin{bmatrix} \hat{\boldsymbol{n}}_0 \\ \vdots \\ \boldsymbol{s}_g + \hat{\boldsymbol{n}}_q \\ \vdots \\ \hat{\boldsymbol{n}}_{Q-1} \end{bmatrix} \tag{60}$$

if the matrices are orthogonal. In (60), $\hat{\boldsymbol{n}}_q = \boldsymbol{A}_q^H \tilde{\boldsymbol{n}}_g$. Explicitly, only the activated index contains both signals and noise, while all the others contain only noise. Then the signs of all elements in $\hat{\boldsymbol{z}}$ are converted to positive to obtain a folded $\hat{\boldsymbol{z}}_{fold}$. Based on $\hat{\boldsymbol{z}}_{fold}$, a joint MLD can be executed to obtain $\hat{q}$ and $\hat{\boldsymbol{s}}_{g,fold}$, which can be expressed as

$$(\hat{q}, \hat{\boldsymbol{s}}_{g,fold}) = \underset{q\in\mathcal{Q}, \boldsymbol{s}_{g,fold}\in\mathcal{M}_{1/4}^{N_g}}{\arg\min} ||\hat{\boldsymbol{z}}_{fold} - \boldsymbol{s}_{fold}||^2. \tag{61}$$

Note that, in (61), the length of $\boldsymbol{s}_{fold}$ matches to that of $\boldsymbol{z}_{fold}$, and the index q determines the locations of the N_g folded symbols in $\boldsymbol{s}_{g,fold}$. Finally, following the description in Subsection III-B1, after converting the signs of $\hat{\boldsymbol{s}}_{gfold}$ to the same signs of the symbols in $\boldsymbol{z}_{\hat{q}}$, N_g m-QAM symbols can be detected.

C. LOW-COMPLEXITY TWO-STAGE IM-QAM DETECTOR (TSD)

The TSD detects the IM symbol and QAM symbols in two stages. During the first stage, the index symbol is detected. Based on the detected result, the QAM symbols are then detected during the second stage.

1) TSD FOR SPIM

Assume that among the N_g positions available for QAM symbol transmission, n positions are activated. After obtaining $\boldsymbol{z}_g$ as expressed in (53) for group g, the power of each symbol position in $\boldsymbol{z}_g$ is computed. The n positions with the highest power can be considered as the positions with QAM symbols, enabling the detection of the index $\hat{q}$. Subsequently, in the second stage, the n transmitted QAM/PSK symbols are detected based on the observed data.

2) TSD FOR SMIM

The TSD in the SMIM scheme also detects the IM symbol and QAM symbols in two stages. During the first stage, the IM symbol is detected. The QAM symbols are detected during the second stage based on the detected results of the first stage. In particular, in the first stage, TSD detects the IM symbol by forming the decision variables described below. First, it processes $\boldsymbol{z}_g$, $g = 0, 1, \ldots, G-1$, shown in (55), using the processing matrices $\boldsymbol{W}_q$, $q = 0, 1, \ldots, Q-1$, as

$$\hat{\boldsymbol{z}}_q = \boldsymbol{W}_q^H \boldsymbol{z}_g,\ q = 0, 1, \ldots, Q-1, \tag{62}$$

where $\boldsymbol{W}_q$ can be constructed as the MF, ZF or MMSE as follows:

$$\begin{aligned} \text{MF}:\ & \boldsymbol{W}_q = \boldsymbol{A}_q, \\ \text{ZF}:\ & \boldsymbol{W}_q = \boldsymbol{A}_q \left(\boldsymbol{A}_q^H \boldsymbol{A}_q\right)^{-1}, \\ \text{MMSE}:\ & \boldsymbol{W}_q = \boldsymbol{A}_q \left(\boldsymbol{A}_q \boldsymbol{A}_q^H + \boldsymbol{R}_{n_g}\right)^{-1}, \end{aligned} \tag{63}$$

TABLE 3. Complexity of MLD, SMLD and TSD in SPIM, SMIM and JMSIM Schemes

	MLD	SMLD	TSD
SPIM	$\mathcal{O}(M^n QG)$	$\mathcal{O}\left(\left(\frac{M}{4}\right)^n QG\right)$	$\mathcal{O}(nQG + nMG)$
SMIM	$\mathcal{O}(M^{N_g} QG)$	$\mathcal{O}\left(\left(\frac{M}{4}\right)^{N_g} QG\right)$	$\mathcal{O}(N_g QG + N_g MG)$
JMSIM	$\mathcal{O}(M^n Q_c Q_s G)$	$\mathcal{O}\left(\left(\frac{M}{4}\right)^n Q_c Q_s G\right)$	$\mathcal{O}(nQ_c Q_s G + nMG)$

where $\boldsymbol{R}_{n_g} = E[\boldsymbol{n}_g \boldsymbol{n}_g^H]$ is the noise covariance matrix. Second, TSD forms Q decision variables as

$$Z_q = \|\hat{\boldsymbol{z}}_q\|^2,\ q = 0, 1, \ldots, Q-1. \tag{64}$$

Finally, the index symbol is detected as $\hat{q} = \arg\max_q \{Z_0, Z_1, \ldots, Z_{Q-1}\}$.

After the detection of the index $\hat{q}$, we obtain the observations for detecting QAM symbols as

$$\hat{\boldsymbol{z}}_{\hat{q}} = \boldsymbol{W}_{\hat{q}}^H \boldsymbol{z}_g. \tag{65}$$

Normalizing it using $\boldsymbol{\Gamma} = \text{diag}(\boldsymbol{W}_{\hat{q}}^H \boldsymbol{A}_q)$, we obtain

$$\bar{\boldsymbol{z}}_{\hat{q}} = \boldsymbol{\Gamma}^{-1} \boldsymbol{W}_{\hat{q}}^H \boldsymbol{z}_g, \tag{66}$$

based on which the N_g QAM symbols are detected.

D. DETECTION COMPLEXITY ANALYSIS

As examples, we analyze and compare the complexity of the MLD, SMLD, and TSD for the SMIM scheme. Specifically, one user transmitting M-QAM symbols is assumed.

In the MLD, the number of possible combinations of a symbol vector is M^{N_g}. When there are Q index matrices and G groups, the detector needs to compare $M^{N_g} QG$ times, giving the complexity of $\mathcal{O}(M^{N_g} QG)$.

For SMLD, the number of possible combinations of a symbol vector becomes $(\frac{M}{4})^{N_g}$ because the folded constellation is used. Hence the complexity is $\mathcal{O}((\frac{M}{4})^{N_g} QG)$.

Finally, for TSD, there are only Q vectors to compare, each of which has N_g symbols. Hence, to identify the matrix index for a user, the detector only needs to compare $N_g QG$ times. The M-QAM detection has a detection complexity of $\mathcal{O}(M)$. Hence, the complexity of TSD is $\mathcal{O}(N_g QG + N_g MG)$, which is much lower than that of the SMLD and MLD.

Note that, with n activated symbol positions in both SPIM and JMSIM, there are Q_c matrix indices and Q_s symbol indices in JMSIM.

The complexity of MLD, SMLD and TSD in the context of the three modulation schemes are summarized in Table 3.

IV. PERFORMANCE RESULTS AND DISCUSSION

In this section, we present the simulation results of the considered schemes, where the parameters used in simulations are listed in Table 4. In our performance studies, the maximum decomposition factor of WT is set to $J_m = \log_2(N)$. All of the wavelet functions with $J \le J_m$ are employed for subcarrier signaling. Specifically, the maximum decomposition factors of $\boldsymbol{\mathcal{W}}_N$ and $\boldsymbol{\mathcal{W}}_U$ are set to $J_N = 5$ and $J_U = 6$, respectively. Furthermore, the Haar wavelet is used as the basis function

TABLE 4. Simulation Parameters

Parameters	Value
Number of total subcarriers	$U = 64$
Number of users	$K = 2$
Number of subcarriers per user	$N = 32$
Number of groups	$G = 2$ or 4
Number of subcarriers per group	$N_g = 16$ or 8
Number of BPS	$B = 36$
Number of channel paths	$L = 6$

TABLE 5. Configurations of SPIM, SMIM and JMSIM Schemes for Attaining the Same Throughput

	$N_g = 16$			$N_g = 8$		
	n	**Modulation**	Q	n	**Modulation**	Q
SPIM	2	64QAM	1	1	64QAM	1
SMIM	16	BPSK	4	8	BPSK	2
JMSIM	1	16QAM	1024	1	8QAM	8

of WT. To ensure that the dispersion matrices have near orthogonality, the size of the matrix needs to be relatively large. According to our simulations, when the size of the dispersion matrices is not smaller than 16×16, the matrices do not affect the simulation results significantly owing to the near orthogonality. However, if the size of the dispersion matrices is relatively small, the Gram-Schmidt matrix orthogonalization needs to be executed to obtain the needed orthogonality.

To ensure a fair comparison of the different schemes, we set the SPIM, SMIM and JMSIM systems to have the same throughput of $B = 36$ BPS, as shown in Table 4. Then, we set different combinations for the number of selected symbol positions n, the modulation order M and the number of code matrices Q, as shown in Table 5, to achieve the same throughput of B under different values of N_g.

First, Fig. 7 compares the BER performance of the proposed SC-FDMA system using, respectively, the SPIM, SMIM and JMSIM schemes with $N_g = 16$, while employing the dispersion matrices by the method in Section II-E-1 or the GS matrices by the method in Section II-E-2, as well as the various detection schemes. Furthermore, in Fig. 7(a), the performance of the SPIM-assisted SC-FDMA systems with the dispersion matrix or GS matrix is compared with that of the SC-FDMA systems using the Walsh Hadamard matrix [53] as spreading matrix. Additionally, in Fig. 7(a), the performance attained by the proposed schemes is also compared with that of the conventional IM scheme [36], [37], which implements IM at subcarrier level to obtain the same throughput as the other schemes considered. Note that, in Fig. 7(a), all the curves corresponding to the conventional IM and the Walsh Hadamard matrix are overlapping with each other. Note additionally that, due to its fixed structure, the Walsh Hadamard matrix is not sufficient for the implementation of SMIM and JMSIM, as both of them require multiple matrices to implement the matrix-based IM.

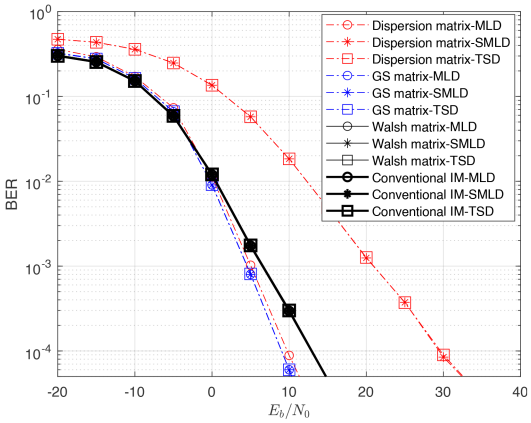

(a) SPIM

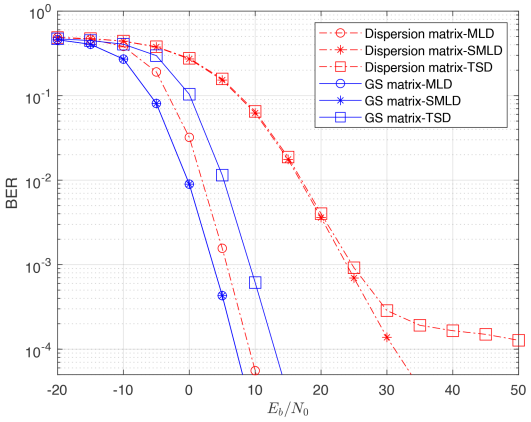

(b) SMIM

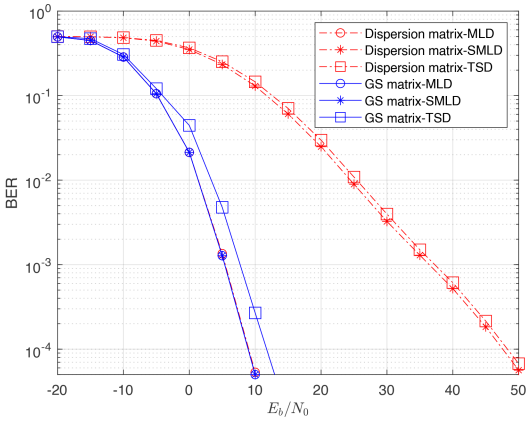

(c) JMSIM

FIGURE 7. BER performances of the SPIM, SMIM and JMSIM schemes with random dispersion matrix and Gram-Schmidt orthogonalized matrix, when various detection schemes are considered.

As shown in Fig. 7, for SPIM, SMIM, and JMSIM, the GS derived matrices can provide better BER performance than the randomly generated Gaussian dispersion matrices and the Walsh Hadamard matrix. The results indicate that the orthogonality and appropriate Gaussian distribution of the GS matrices facilitate the detection of the spreading matrix in SMIM and JMSIM, while also enhancing the performance of

code matrix elimination in SPIM. This is more evident when SMLD and TSD are employed. For example, as shown in Fig. 7(a), the elimination of the SPIM scheme with both SMLD and TSD assisted by GS matrices is significantly better than that using the random Gaussian dispersion matrices, yielding a gain of about 20 dB at a BER of 10^{-4} . Accordingly, when SMIM or JMSIM is employed, the gain is about 20 dB or 25 dB, as shown in Fig. 7(b) and (c). Moreover, the results show that the SMLD applied in SMIM and JMSIM schemes slightly outperforms the TSD, when employing the GS generated matrices. In comparison with the constant code matrix in SPIM, the multiple options of spreading matrices in SMIM and JMSIM introduce more errors in the index detection. However, the symbol vector in JMSIM has only few activated symbols. Hence, the apparent power gap between these active symbol positions and other positions without symbols makes the index detection easier in TSD. Correspondingly, as seen in Fig. 7, the performance of the JMSIM scheme with TSD is slightly better than that of the SMIM scheme with TSD.

Additionally, as shown in Fig. 7(a), except the case of MLD, the performance of the SC-FDMA using Walsh Hadamard matrix [53] is better than that of the SC-FDMA using dispersion matrix, but always worse than that of the SC-FDMA employing GS matrix. This is can be explained as follows. In Walsh Hadamard matrix, all elements possess equal modulus, which uniformly distribute a symbol over all the subcarriers, implementing the same function as the FFT operation in the conventional SC-FDMA. Owing to its orthogonality, a similar BER performance can be obtained for different detection schemes considered. By contrast, the elements of GS matrix exhibit Gaussian distribution. The non-uniform weightings of symbol distribution across subcarriers provide additional gain, thus leading to an improved BER performance.

Fig. 8 compares the BER performance of the proposed system employing the SPIM, SMIM and JMSIM schemes, respectively, with MLD, SMLD or TSD, when the GS matrices with the size $N_g = 8$ and $N_g = 16$ are considered. Note that, the parameters for the Cases 1(a) and 1(b) in Fig. 8(a) are the same as that for Fig. 8(b) and (c). The comparison of these cases with Cases 2 and 3 in Fig. 8(a) will be detailed later. By comparing the BER results of the Cases 1(a/b) in Fig. 8(a) and that in Fig. 8(b) and (c), it can be seen that the matrix size only affects the BER performance of TSD, when the SMIM is employed, as shown in Fig. 8(b). Specifically, at the BER of 10^{-4}, the performance gain achieved by the TSD with $N_g = 16$ is about 5 dB over that by the TSD with $N_g = 8$. This is because the SMIM fully activates the symbol vector, making a larger matrix be able to attain a higher diversity gain. By contrast, in the SPIM and JMSIM schemes, there is only 1 or 2 positions of a symbol vector activated, as shown in Table 5. In this case, even when the 8×8 matrices are used, full diversity gain cannot be achieved. As shown in Fig. 8, when MLD or SMLD is employed, the SMIM scheme outperforms the SPIM and JMSIM scheme, which is as expected. More specifically,

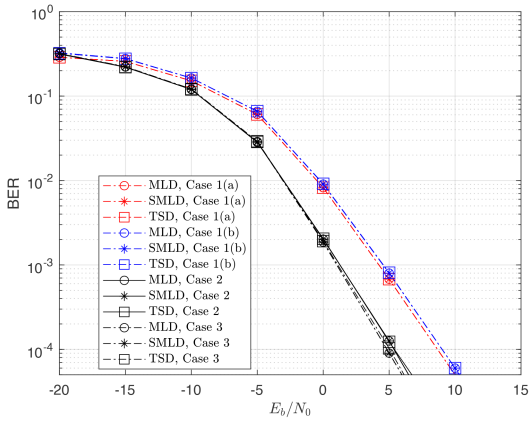

(a) SPIM with N_g = 8 and 16.

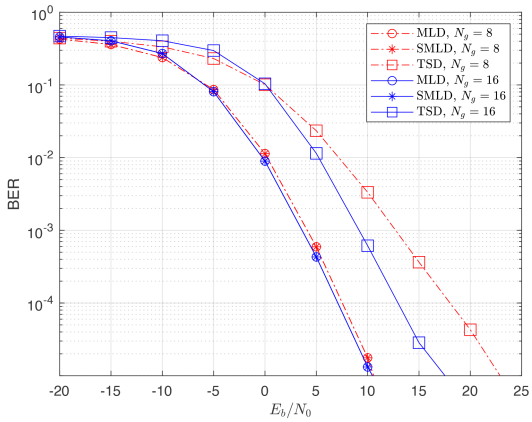

(b) SMIM with N_g = 8 and 16.

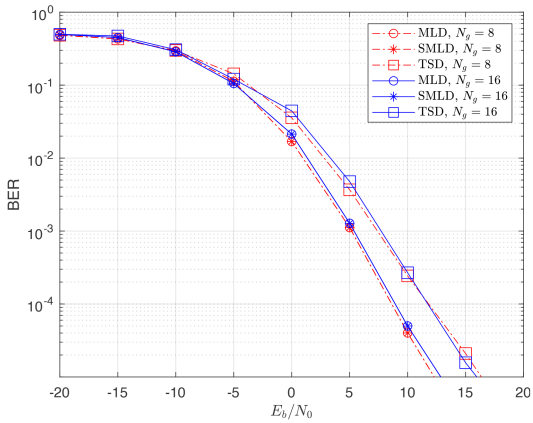

(c) JMSIM with N_g = 8 and 16.

FIGURE 8. BER performance of the proposed systems with Gram- Schmidt orthogonalized matrices for different value of N_g in the SPIM, the SMIM and the JMSIM schemes.

to ensure the same throughput as shown in Table 5, both the SPIM and JMSIM schemes need to use the QAM/PSK modulation of high order. Specifically, the SPIM and JMSIM schemes have to use 64QAM and 16QAM, respectively, when $N_g = 16$. By contrast, for the same throughput, the SMIM scheme only needs to use BPSK, which yields significantly better BER performance.

TABLE 6. Parameters for Demonstrating the Scalability of SC-FDMA System With Different Detection Schemes

Parameters	Case 1(a/b)	Case 2	Case 3
U	64	128	128
K	2	2	4
N	32	64	32
G	4/2	4	2
N_g	8/16	16	16
n	1/2	2	2
Modulation	64QAM	64QAM	64QAM
B	36	72	72
L	6	11	11

All the above performance results are obtained from the same system setting of $U = 64$ subcarriers. To demonstrate the scalability, taking the SPIM scheme as an example, in Fig. 8(a), we compare the BER performance of our SC-FDMA systems with different system sizes. In detail, the parameters used in our simulations are listed in Table 6. Specifically, Case 1(a) and Case 1(b) are that considered in the above performance figures. In Cases 2 and 3, the system bandwidth is twice that in the Case 1. Correspondingly, the total data rate in Cases 2 and 3 is twice the total rate in Cases 1. In Case 2, the number of users is 2, while it is 4 in Case 3. The other parameters are set to satisfy these requirements. Note that, as the system bandwidth in Cases 2 and 3 is twice that in Case 1, when given the channel delay spread generating $L = 6$ paths in Case 1, the number of paths in Cases 2 and 3 is about $L = 11$, according to the formula of $L = [T_m W] + 1$, where T_m is channel's delay spread and W is system bandwidth. From the results of Fig. 8(a), we can observe that, as the system becomes larger, the BER performance slightly improves, which follows the general observation of wireless communication systems. Specifically in the current cases, as the system bandwidth is doubled, the diversity gain increases, owing to the increased number of channel paths. The results of Fig. 8(a) show that Case 3 slightly outperforms Case 2 in high SNR region. This is mainly because the intra-user interference in the Case 2, which sets $N = 64$, is slightly larger than that in the Case 3, which uses $N = 32$.

As illustrated in Fig. 9, the proposed WT-based system is compared with the FFT-based system under three detection methods, namely MLD, SMLD, and TSD, when the SPIM with $N_g = 16$ is considered. Both systems exhibit similar BER performance for all detection methods, which is also shown in Fig. 8(a). However, the WT-based system demonstrates a notable advantage, achieving approximately 5 dB better performance than the FFT-based system at the BER level of 10^{-4}. This improvement stems from the ability of WT to better capture local variations in time-domain signals, a capability attributed to the localized nature of its basis functions and its multiscale transformation approach. By offering high-resolution analysis in both time and frequency-domains, the WT effectively detects transient features and frequency shifts in the signal, thereby enhancing detection accuracy and reducing the BER.

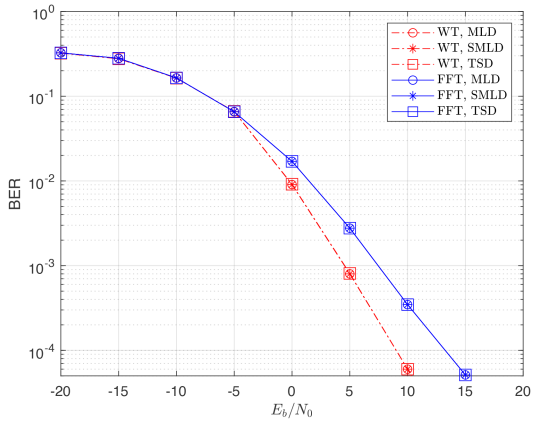

FIGURE 9. BER performance comparison of the proposed WT-based system and the FFT-based system, when MLD, SMLD and TSD in SPIM scheme are respectively employed.

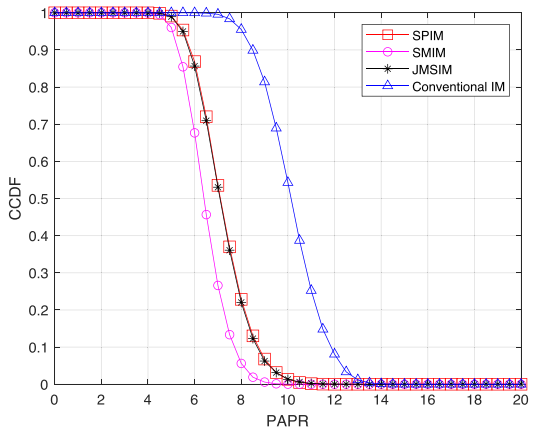

FIGURE 10. PAPR performance attained respectively by the SPIM, SMIM and JMSIM schemes in comparison with that by the conventional IM in the WT-assisted SC-FDMA systems.

Finally, Fig. 10 compares the PAPR performances of the SPIM, SMIM and JMSIM schemes applied to the WT-assisted SC-FDMA, where the PAPR of the WT-assisted SC-FDMA with conventional IM is provided as a benchmark. It can be seen that the employment of spreading matrices can provide an improved PAPR performance. All the three schemes yield significantly lower PAPR to the WT-assisted SC-FDMA than the conventional IM does. In particular, the PAPR performance provided by the SMIM scheme is the best, as the result it activates all symbols, which makes the power distribution over frequency band more uniform, when compared to the SPIM and JMSIM schemes.

V. CONCLUSION

In this paper, we proposed three IM schemes for WT-assisted SC-FDMA systems. The PAPR performance comparison of these IM schemes with the conventional benchmark IM

schemes shows that all the three proposed IM schemes are able to provide lower PAPR. We compared the BER performance of the WT-assisted SC-FDMA systems with the three IM schemes supported by GS matrix and random dispersion matrix. The simulation results demonstrate that the GS matrix is able to provide significant performance improvement over the random dispersion matrix. Furthermore, based on the WT-assisted SC-FDMA system model, we proposed a low-complexity TSD method and compared its resultant BER performance with the other two detection methods, namely MLD and SMLD, with higher complexity. The results show that the TSD method is able to achieve similar or even the same BER performance as the higher-complexity MLD and SMLD methods, when GS matrices are employed. Owing to the above-mentioned advantages, the WT-assisted SC-FDMA using the proposed GS matrices based IM and low-complexity TSD constitutes a promising scheme for supporting the uplink transmission of low-power communication terminals. As a future research issue, sparse matrices may be introduced to replace the dispersion or GS matrices, with information detected at receiver by the message-passing algorithm or approximated message-passing algorithm [54], [55], [56].

REFERENCES

[1] I. Holguin and S. M. Errapotu, "Smart home IoT communication protocols and advances in their security and interoperability," in *Proc. 7th Cyber Secur. Netw. Conf.*, 2023, pp. 208–211.

[2] J. Lorincz and Z. Klarin, "How trend of increasing data volume affects the energy efficiency of 5G networks," *Godišnjak Akademije Tehničkih Znanosti Hrvatske*, vol. 2023, no. 1, pp. 289–306, 2023.

[3] V. Leung, A. G. Burr, L. Song, Y. Zhang, and T. M. Bohnert, "OFDMA architectures, protocols, and applications," *EURASIP J. Wireless Commun. Netw.*, vol. 2009, no. 1, pp. 1–4, 2009.

[4] T. Jiang, D. Chen, C. Ni, and D. Qu, *OQAM/FBMC for Future Wireless Communications: Principles, Technologies and Applications*. New York, NY, USA: Academic, 2017.

[5] K. K. Vaigandla, M. Siluveru, and S. R. Bolla, "Analysis of PAPR and beamforming for 5 G MIMO-OFDM," *Int. J. Anal. Exp. Modal Anal.*, vol. 12, pp. 483–490, 2020.

[6] H. G. Myung and D. J. Goodman, *Single Carrier FDMA: A New Air Interface for Long Term Evolution*. Hoboken, NJ, USA: Wiley, 2008.

[7] H. G. Myung, J. Lim, and D. J. Goodman, "Peak-to-average power ratio of single carrier FDMA signals with pulse shaping," in *Proc. IEEE 17th Int. Symp. Pers., Indoor Mobile Radio Commun.*, 2006, pp. 1–5.

[8] H. G. Myung, "Introduction to single carrier FDMA," in *Proc. 15th Eur. Signal Process. Conf.*, 2007, pp. 2144–2148.

[9] M. H. Owaid and S. J. Mohammed, "PAPR performance analysis of SC-FDMA and SC-FDMA-DSCDMA," in *Proc. 8th Int. Conf. Contemporary Inf. Technol. Math.*, 2022, pp. 284–289.

[10] H. G. Myung, J. Lim, and D. J. Goodman, "Single carrier FDMA for uplink wireless transmission," *IEEE Veh. Technol. Mag.*, vol. 1, no. 3, pp. 30–38, Sep. 2006.

[11] J. Gazda, P. Drotár, P. Galajda, and D. Kocur, "Comparative evaluation of OFDMA and SC-FDMA based transmission systems," in *Proc. IEEE 8th Int. Symp. Appl. Mach. Intell. Informat.*, 2010, pp. 177–181.

[12] C. A. Azurdia-Meza, K. Lee, and K. Lee, "PAPR reduction in SC-FDMA by pulse shaping using parametric linear combination pulses," *IEEE Commun. Lett.*, vol. 16, no. 12, pp. 2008–2011, Dec. 2012.

[13] K. K. Vaigandla and D. N. Venu, "BER, SNR and PAPR analysis of OFDMA and SC-FDMA," *GIS Sci. J.*, vol. 8, no. 9, pp. 970–977, 2021.

[14] D. Karamehmedovic, M. K. Lakshmanan, and H. Nikookar, "Optimal wavelet design for multicarrier modulation with time synchronization error," in *Proc. IEEE Glob. Telecommun. Conf.*, 2009, pp. 1–6.

[15] S. Baig, M. Ahmad, H. M. Asif, M. N. Shehzad, and M. H. Jaffery, "Dual PHY layer for non-orthogonal multiple access transceiver in 5G networks," *IEEE Access*, vol. 6, pp. 3130–3139, 2018.

[16] A. Khan, S. Baig, and T. Nawaz, "DWMT transceiver equalization using overlap FDE for downlink ADSL," *Turkish J. Elect. Eng. Comput. Sci.*, vol. 23, no. 3, pp. 681–697, 2015.

[17] A. Khan, A. Arif, T. Nawaz, and S. Baig, "Walsh Hadamard transform based transceiver design for SC-FDMA with discrete wavelet transform," *China Commun.*, vol. 14, no. 5, pp. 193–206, 2017.

[18] E. Basar, M. Wen, R. Mesleh, M. Di Renzo, Y. Xiao, and H. Haas, "Index modulation techniques for next-generation wireless networks," *IEEE Access*, vol. 5, pp. 16693–16746, 2017.

[19] M. Di Renzo, H. Haas, A. Ghrayeb, S. Sugiura, and L. Hanzo, "Spatial modulation for generalized MIMO: Challenges, opportunities, and implementation," *Proc. IEEE*, vol. 102, no. 1, pp. 56–103, Jan. 2014.

[20] N. Ishikawa, S. Sugiura, and L. Hanzo, "50 years of permutation, spatial and index modulation: From classic RF to visible light communications and data storage," *IEEE Commun. Surveys Tuts.*, vol. 20, no. 3, pp. 1905–1938, Thirdquarter 2018.

[21] X. Cheng, M. Zhang, M. Wen, and L. Yang, "Index modulation for 5G: Striving to do more with less," *IEEE Wireless Commun.*, vol. 25, no. 2, pp. 126–132, Apr. 2018.

[22] S. Sugiura, T. Ishihara, and M. Nakao, "State-of-the-art design of index modulation in the space, time, and frequency domains: Benefits and fundamental limitations," *IEEE Access*, vol. 5, pp. 21774–21790, 2017.

[23] P. Yang, M. Di Renzo, Y. Xiao, S. Li, and L. Hanzo, "Design guidelines for spatial modulation," *IEEE Commun. Surveys Tuts.*, vol. 17, no. 1, pp. 6–26, Firstquarter 2015.

[24] T. Mao, Q. Wang, Z. Wang, and S. Chen, "Novel index modulation techniques: A survey," *IEEE Commun. Surveys Tuts.*, vol. 21, no. 1, pp. 315–348, Firstquarter 2019.

[25] M. Wen et al., "A survey on spatial modulation in emerging wireless systems: Research progresses and applications," *IEEE J. Sel. Areas Commun.*, vol. 37, no. 9, pp. 1949–1972, Sep. 2019.

[26] Y. A. Chau and S.-H. Yu, "Space modulation on wireless fading channels," in *Proc. IEEE 54th Veh. Technol. Conf. VTC Fall*, 2001, vol. 3, pp. 1668–1671.

[27] R. Mesleh, H. Haas, C. W. Ahn, and S. Yun, "Spatial modulation—A new low complexity spectral efficiency enhancing technique," in *Proc. 1st Int. Conf. Commun. Netw. China*, 2006, pp. 1–5.

[28] R. Y. Mesleh, H. Haas, S. Sinanovic, C. W. Ahn, and S. Yun, "Spatial modulation," *IEEE Trans. Veh. Technol.*, vol. 57, no. 4, pp. 2228–2241, Jul. 2008.

[29] S. Jacob, T. L. Narasimhan, and A. Chockalingam, "Space-time index modulation," in *Proc. IEEE Wireless Commun. Netw. Conf.*, 2017, pp. 1–6.

[30] E. Başar, Ü. Aygölü, E. Panayirci, and H. V. Poor, "Orthogonal frequency division multiplexing with index modulation," *IEEE Trans. Signal Process.*, vol. 61, no. 22, pp. 5536–5549, Nov. 2013.

[31] Y. Xiao, S. Wang, L. Dan, X. Lei, P. Yang, and W. Xiang, "OFDM with interleaved subcarrier-index modulation," *IEEE Commun. Lett.*, vol. 18, no. 8, pp. 1447–1450, Aug. 2014.

[32] R. Fan, Y. J. Yu, and Y. L. Guan, "Generalization of orthogonal frequency division multiplexing with index modulation," *IEEE Trans. Wireless Commun.*, vol. 14, no. 10, pp. 5350–5359, Oct. 2015.

[33] X. Cai et al., "Toward RIS-aided non-coherent communications: A joint index keying M-ary differential chaos shift keying system," *IEEE Trans. Wireless Commun.*, vol. 22, no. 12, pp. 9045–9062, Dec. 2023.

[34] X. Cai, W. Xu, L. Wang, and G. Kaddoum, "Joint energy and correlation detection assisted non-coherent OFDM-DCSK system for underwater acoustic communications," *IEEE Trans. Commun.*, vol. 70, no. 6, pp. 3742–3759, Jun. 2022.

[35] X. Cai, C. Yuen, C. Huang, W. Xu, and L. Wang, "Toward chaotic secure communications: An RIS enabled M-ary differential chaos shift keying system with block interleaving," *IEEE Trans. Commun.*, vol. 71, no. 6, pp. 3541–3558, Jun. 2023.

[36] J. Manco-Vasquez, M. Chafii, and F. Bader, "Tailoring index-modulation for uplink IoT and M2M networks," in *Proc. IEEE Wireless Commun. Netw. Conf.*, 2019, pp. 1–6.

[37] M. B. Shahab, S. J. Johnson, M. Shirvanimoghaddam, M. Chafii, E. Basar, and M. Dohler, "Index modulation aided uplink NOMA for massive machine type communications," *IEEE Wireless Commun. Lett.*, vol. 9, no. 12, pp. 2159–2162, Dec. 2020.

[38] M. Chafii, F. Bader, and J. Palicot, "SC-FDMA with index modulation for M2M and IoT uplink applications," in *Proc. IEEE Wireless Commun. Netw. Conf.*, 2018, pp. 1–5.

[39] D. F. Walnut, *An Introduction to Wavelet Analysis*. Berlin, Germany: Springer, 2013.
[40] Z. Tang and S. Cheng, "Interference cancellation for DS-CDMA systems over flat fading channels through pre-decorrelating," in *Proc. 5th IEEE Int. Symp. Pers., Indoor Mobile Radio Commun., Wireless Networks - Catching Mobile Future*, 1994, vol. 2, pp. 435–438.
[41] C. Douillard et al., "Iterative correction of intersymbol interference: Turbo-equalization," *Eur. Trans. Telecommun.*, vol. 6, no. 5, pp. 507–511, 1995.
[42] N. J. Fliege, *Multirate Digital Signal Processing: Multirate Systems, Filter Banks, Wavelets*. Hoboken, NJ, USA: Wiley, 1994.
[43] A. Khan, S. Khan, S. Baig, H. M. Asif, and S. Y. Shin, "Wavelet OFDM with overlap FDE for non-Gaussian channels in precoded NOMA based systems," *Future Gener. Comput. Syst.*, vol. 97, pp. 165–179, 2019. [Online]. Available: https://www.sciencedirect.com/science/article/pii/S0167739X18318272
[44] R. S. Pathak, *The Wavelet Transform*, vol. 4. Berlin, Germany: Springer, 2009.
[45] L.-L. Yang, *Multicarrier Communications*. Hoboken, NJ, USA: Wiley, 2009.
[46] R. Zhang, L.-L. Yang, and L. Hanzo, "Generalised pre-coding aided spatial modulation," *IEEE Trans. Wireless Commun.*, vol. 12, no. 11, pp. 5434–5443, Nov. 2013.
[47] X. Cai, C. Huang, P. Chen, E. Basar, and C. Yuen, "Design of non-coherent RIS-empowered DCSK with two-level nested index modulation," *IEEE Trans. Wireless Commun.*, vol. 24, no. 4, pp. 3044–3058, Apr. 2025.
[48] S. Sugiura, S. Chen, and L. Hanzo, "Coherent and differential space-time shift keying: A dispersion matrix approach," *IEEE Trans. Commun.*, vol. 58, no. 11, pp. 3219–3230, Nov. 2010.
[49] S. X. Ng and L. Hanzo, "On the MIMO channel capacity of multidimensional signal sets," *IEEE Trans. Veh. Technol.*, vol. 55, no. 2, pp. 528–536, Mar. 2006.
[50] L.-L. Yang, J. Shi, K.-T. Feng, L.-H. Shen, S.-H. Wu, and T.-S. Lee, *Resource Optimization in Wireless Communications: Fundamentals, Algorithms, and Applications*. New York, NY, USA: Academic, 2025.
[51] S. J. Leon, Å. Björck, and W. Gander, "Gram-Schmidt orthogonalization: 100 years and more," *Numer. Linear Algebra Appl.*, vol. 20, no. 3, pp. 492–532, 2013.
[52] S. Sugiura, C. Xu, S. X. Ng, and L. Hanzo, "Reduced-complexity coherent versus non-coherent QAM-aided space-time shift keying," *IEEE Trans. Commun.*, vol. 59, no. 11, pp. 3090–3101, Nov. 2011.
[53] X. Cai, Z. Xie, P. Chen, Y. Fang, E. Basar, and C. Yuen, "Quadruple code index modulation," *IEEE Trans. Cogn. Commun. Netw.*, early access, Dec. 11, 2024, doi: 10.1109/TCCN.2024.3516050.
[54] Y. Liu, L.-L. Yang, and L. Hanzo, "Spatial modulation aided sparse code-division multiple access," *IEEE Trans. Wireless Commun.*, vol. 17, no. 3, pp. 1474–1487, Mar. 2018.
[55] Y. Liu, L.-L. Yang, P. Xiao, H. Haas, and L. Hanzo, "Spatial modulated multicarrier sparse code-division multiple access," *IEEE Trans. Wireless Commun.*, vol. 19, no. 1, pp. 610–623, Jan. 2020.
[56] Y. Liu, L. Xiang, L.-L. Yang, and L. Hanzo, "Space-time coded generalized spatial modulation for sparse code division multiple access," *IEEE Trans. Wireless Commun.*, vol. 20, no. 8, pp. 5359–5372, Aug. 2021.

ZHOU LU received the B.Eng. degree in communications engineering from Xidian University, Xi'an, China, and Heriot-Watt University, Edinburgh, U.K., in 2020, and the M.Sc. degree in wireless communications and smart networking in 2021 from the University of Southampton, Southampton, U.K., where he is currently working toward the Ph.D degree. His research interests include multicarrier communications and affine frequency division multiplexing in high-mobility wireless communications.

MOHAMMED EL-HAJJAR (Senior Member, IEEE) is currently a Professor of signal processing for wireless communications with the School of Electronics and Computer Science, University of Southampton, Southampton, U.K. He has authored or coauthored a Wiley-IEEE book and more than 100 IEEE journal and conference papers and in excess of 10 patents.His research interests include design of intelligent and energy-efficient transceivers, MIMOs, millimeter wave communications, and machine learning for wireless communications. His research was funded by the Engineering and Physical Sciences Research Council, Royal Academy of Engineering, and many industrial partners. He was the recipient of several academic awards.

LIE-LIANG YANG (Fellow, IEEE) received the M.Eng. and Ph.D. degrees in communications and electronics from Northern (Beijing) Jiaotong University, Beijing, China, in 1991 and 1997, respectively, and the B.Eng. degree in communications engineering from Shanghai TieDao University, Shanghai, China, in 1988. He is currently a Professor of wireless communications with the School of Electronics and Computer Science, University of Southampton, Southampton, U.K. He has authored or coauthored more than 500 research papers in journals and conference proceedings, authored or coauthored four books and more than ten chapters. His research interests include wireless communications, wireless networks and signal processing for wireless communications, molecular communications, and nano-networks. He is also a Fellow of IET, AAIA and AIIA, and was a Distinguished Lecturer of IEEE VEHICULAR TECHNOLOGY SOCIETY. He has served various roles for some research journals, and acted different roles for organization of conferences.